

1 **Modulation of the Substorm Current Wedge by Bursty Bulk Flows: September 8,**
2 **2002 - Revisited**
3

4 **L. Palin¹, H. J. Opgenoorth¹, K. Ågren¹, T. Zivkovic¹, V. A. Sergeev³, M. V. Kubyshkina³,**
5 **A. Nikolaev³, K. Kauristie², M. van de Kamp², O. Amm (POSTHUM)², S. E. Milan⁴, S. M.**
6 **Imber⁴, G. Facskó^{2,6}, M. Palmroth², R. Nakamura⁵**

7 ¹Swedish Institute of Space Physics, Uppsala, Sweden.

8 ²Finnish Meteorological Institute, Earth Observational Unit, Helsinki, Finland.

9 ³St. Petersburg State University, Physics Faculty, St. Petersburg, Russia.

10 ⁴Department of Physics and Astronomy, University of Leicester, Leicester, UK.

11 ⁵Space Research Institute, Austrian Academy of Sciences, Graz, Austria.

12 ⁶Geodetic and Geophysical Institute, Research Centre for Astronomy and Earth Sciences,
13 Hungarian Academy of Sciences, Sopron, Hungary.

14
15 Corresponding author: Laurianne Palin (lpalin@irfu.se)

16 **Key Points:**

- 17 • A localized substorm onset current wedge is modulated stepwise
18 • Build up of the SCW is due to a dense sequence of arrival of BBFs in the near-Earth tail
19 • An intense substorm is the result of a group or sequence of more intense and more
20 frequent BBFs
21

22 Abstract

23 The ultimate formation mechanism of the substorm current wedge (SCW) remains to-date
24 unclear. In this study, we investigate its relationship to plasma flows at substorm onset and
25 throughout the following expansion phase. We revisit the case of September 8, 2002, which has
26 been defined as “one of the best textbook examples of a substorm” because of its excellent
27 coverage by both spacecraft in the magnetotail and ground-based observatories. We found that a
28 dense sequence of arrival of nightside flux transfer events (NFTEs, which can be understood as
29 the lobe magnetic signature due to a bursty bulk flow travelling earthward in the central
30 plasmashet) in the near-Earth tail leads to a modulation (and further step-like built-up) of the
31 SCW intensity during the substorm expansion phase. In addition, we found that small SCWs are
32 created also during the growth phase of the event in association with another less intense
33 sequence of NFTEs. The differences between the sequence of NFTEs in the growth and
34 expansion phase are discussed. We conclude that the envelope of the magnetic disturbances
35 which we typically refer to as an intense magnetic substorm is the result of a group or sequence
36 of more intense and more frequent NFTEs.

37 1 Introduction

38 The original concept of auroral (and later magnetospheric) substorms was introduced by
39 *Akasofu* [1964]. The latest definition of the full substorm concept in various regions of geospace
40 has been given by *Angelopoulos et al* [2008]: “substorms are global reconfigurations of the
41 magnetosphere involving storage of solar wind energy in the Earth’s magnetotail and its abrupt
42 conversion to particle heating and kinetic energy”. They are composed of three parts: growth
43 phase (energy loading in the magnetosphere), expansion phase (release of that stored energy) and
44 recovery phase (return of the magnetosphere to its ground state). The mechanism that triggers
45 the substorm onset itself is still unknown even if some models, which try to explain substorms,
46 have been heavily debated. Particularly current disruption (CD) or magnetic reconnection (MR)
47 at the near Earth neutral line (NENL) [*Lui et al.*, 1996; *Baker et al.*, 1996; *Lui et al.*, 2000] have
48 been advocated as alternative explanations for many observed substorm features. Recently, new
49 observations have emphasized the importance of flow bursts in the central plasma sheet, which
50 may trigger the substorm breakup [*Nishimura et al.*, 2010; *Mende et al.*, 2011], also summarized
51 in *Sergeev et al.* [2012].

52 One of the key signatures of substorms is the localized onset of a three-dimensional
53 current system, generated when the magnetospheric cross-tail current is disrupted and diverted
54 toward the ionosphere by localized field-aligned currents (FAC). This substorm related 3D
55 current system, which couples the magnetosphere to the ionosphere, is usually called the
56 substorm current wedge (SCW) [*Atkinson et al.*, 1967; *McPherron et al.*, 1973, *Kepko et al.*,
57 2014]. It consists of the cross-tail current, a downward FAC at the eastern side of the wedge, an
58 upward FAC at the western side of the wedge, and a connecting westward electrojet in the
59 ionosphere. The magnetic disturbances of this current system on ground level are detectable by
60 ground-based magnetometers at both high [*Oppenoorth et al.*, 1981; *Baumjohann et al.*, 1983]
61 and low latitudes [*McPherron et al.*, 1973]. The method based on low latitude data is better
62 suited to get the overall current pattern and total intensity rather than the local details, as it is not
63 directly affected by the local ionospheric conductivity conditions (the exact distribution of, and
64 the relation between Hall and Pedersen conductances) which determines the high latitude
65 magnetic disturbances. The SCW is typically very narrow at substorm onset, but expands rapidly

66 to east, west and poleward during substorm expansion. It is associated with the dipolarization of
67 the magnetic field in the magnetotail, a sign of a global reconfiguration of the magnetosphere,
68 identified as a long lasting B_z increase in satellite data from that region. Dipolarizations [Nagai,
69 1982] are different from the transient B_z increase associated with localized plasma flows
70 (magnetic pile up associated with local plasma flow), which are called dipolarization fronts (DF)
71 [Nakamura *et al.*, 2002, 2009; Lui *et al.*, 2014].

72 The close relationship between plasma sheet flow bursts and the SCW is highlighted in
73 the recent review of Kepko *et al.*, [2014] taking advantage of both simulations and observational
74 results. The flows carry plasma with reduced entropy and enhanced magnetic flux that penetrate
75 deep into the magnetosphere [Panov *et al.*, 2010 ; Sergeev *et al.*, 2014]. The pressure distribution
76 in the inner magnetosphere deflects the flows, thus creating vortices, magnetic shears and
77 pressure distributions that are associated with field-aligned currents [Birn *et al.*, 1999, 2004;
78 Keiling *et al.*, 2009]. The accumulation of many stopped flow bursts can cause a large-scale
79 pressure buildup responsible for a long-lasting SCW [Birn and Hesse, 2014].

80 Plasma flows brake when entering the inner magnetosphere due to dipolar magnetic field
81 and can “bounce” against this magnetic barrier [Panov *et al.*, 2010]. This “bouncing” is observed
82 as a succession of earthward and tailward flow with a decreasing velocity within a few minutes.
83 Due to the oscillatory flow, a “polarization current” and a current associated with the oscillating
84 part of the pressure gradient are created. Those add to the major current wedge generated by the
85 general reconfiguration of the pressure gradient in the magnetotail [Panov *et al.*, 2013]. The
86 same authors also found that those two alternate currents are responsible for the ~2.5 min-period
87 modulation of the total ionospheric current that was earlier identified as Pi2 pulsations in ground-
88 based measurements of the magnetic field [Olson, 1999, and references therein].

89 Recently, Liu *et al* [2015] proposed a new scenario of SCW formation. Using THEMIS
90 mission data they carried out a statistical study of “wedgelets”, defined as narrow FAC pairs,
91 carried by elemental flux transport units defined as dipolarizing flux bundles (DFBs) [Liu *et al.*,
92 2013]. Their results show characteristic asymmetries in the individual wedgelets: in the dawn
93 (dusk) sector of the magnetotail, a wedgelet has stronger FAC towards (away from) the Earth
94 than away from (towards) the Earth, so the total net FAC at dawn (dusk) is towards (away from)
95 the Earth. They concluded that the combined effect of many wedgelets is thus the same as that of
96 large-scale region-1-sense SCW, supporting the idea that many small wedgelets comprise the
97 large SCW. They point out that when there are only a few DBFs providing few FACs, a so-
98 called *pseudobreakup* is more likely to occur than a full-scale SCW. The term “*pseudobreakup*”
99 was introduced by Akasofu [1964] to describe events with an initial auroral brightening, just like
100 at substorm onset, which, however, subsides a few minutes later without major expansion. If
101 DFBS arrive continuously for several tens of minutes, a long-lasting SCW could thus be
102 sustained by the associated wedgelets. However, a particular weakness of the study by Liu *et al.*
103 [2013] is that it did not consider whether the observed DBFs and wedgelets did, in fact, occur
104 during substorm times or not.

105 The capability of flow bursts to generate a small current wedge, even under relatively
106 quiet conditions, has recently been investigated by Palin *et al.* [2015]. Using Themis data they
107 investigated flow bursts in the magnetotail under quiet solar wind conditions for a period of
108 seven hours preceding a substorm onset. According to the PC-index (polar cap index), this period
109 could be interpreted as a long-lasting growth phase. Eight successive plasma sheet (PS)
110 activations, including DF and bursty bulk flows (BBF) [Angelopoulos *et al.*, 1992], were

111 observed. When observed from the lobes, these PS activations show the magnetic and particle
112 signatures of earthward-contracting recently reconnected flux tubes, i.e. NFTEs (nightside flux
113 transfer events) [Sergeev *et al.*, 1992; 2005]. All PS activations were associated with the
114 formation of a small and localized SCW, as identified in ground-based magnetometer data at
115 auroral and subsuroral latitudes. These current wedges appeared to be the direct consequence of
116 BBF arrival in the near tail independently of the amplitude of the DFs. Unfortunately, in the case
117 study of *Palin et al.* [2015], no data was anymore available at the time of the subsequent
118 substorm onset itself, or throughout the following substorm expansion phase (neither from
119 spacecraft in the tail nor ground-based instruments).

120

121 *Sergeev et al.* [2005] studied a well-isolated substorm observed by a radial configuration of
122 several spacecraft over central Scandinavia, which they defined as a “textbook example of
123 growth/expansion/recovery phases with unprecedented coverage of all basic regions”. During
124 this event two sequences of NFTEs have been identified using magnetic field and particle
125 observations from the Cluster spacecraft. One sequence of NFTEs occurred during the growth
126 phase and the other one at substorm onset and throughout the initial expansion phase. This
127 substorm event study benefits from an exceptionally good coverage by ground-based
128 magnetometers as the footprints of Cluster spacecraft happen to be right above Scandinavia and
129 the Image magnetometer network at the moment of substorm onset (see Figure 1). Therefore, this
130 particular substorm is of great interest for us, as it will allow us to continue our study of the
131 relation between flow burst and SCW in the substorm expansion phase, which was not possible
132 in the previous case study of *Palin et al.*, [2015].

133 As this is such an exceptionally well-instrumented event two other additional papers have
134 already been published on the same period: *Semenov et al.* [2005], and *Keiling et al.* [2006].
135 *Semenov et al.* [2005] used the dataset to test a model of transient time-dependent magnetic
136 reconnection, which is applied to this case study to describe the behavior of NFTEs in the
137 Earth’s magnetotail. Using their model they could deduce the location of the reconnection site,
138 which was located at about 29-31Re in the magnetotail. *Keiling et al.* [2006] returned to this
139 event to study substorm related Pi2 pulsations. The series of NFTEs at substorm onset earlier
140 identified by [Sergeev *et al.* 2005] (from now on referred to as “S05”) has by these authors been
141 interpreted as tail lobe Pi2 pulsations. The first onset of Pi2 pulsation observed on the ground is
142 found to happen only ~30 sec after the related observations in the tail. The authors concluded
143 that the Pi2 pulsations both in space and on the ground are, indeed, remotely driven by pulsed
144 magnetic reconnection, explicitly: “reconnection can be coupled to the ionosphere through what
145 is phenomenologically known as Pi2 pulsations”.

146 The aim of this paper is to revisit the observations of S05, using new data analysis
147 methods and additional data provided by a EU-FP7 funded collaborative data analysis project
148 (see below), in order to investigate the relation between flow bursts and SCW in its expansion
149 phase.

150

151 2 Instruments

152 In this study we used magnetic field and particle data from the Cluster mission [*Escoubet*
153 *et al.*, 2001] provided by the Cluster Active Archive. Spin resolution (4s) data for the magnetic

154 field were obtained from the FluxGate Magnetometer [Balogh *et al.*, 1997, 2001]. The
155 COmposition and DIstribution Function sensor (CODIF) [Rème *et al.*, 1997, 2001] provided the
156 ion data. We also used the magnetic data from POLAR [Russell *et al.*, 1995] and Geotail
157 [Kokubun *et al.*, 1994] spacecraft, and data from the Imager for Magnetopause-to-Aurora Global
158 Exploration (IMAGE) [Gibson *et al.*, 2000].

159 Ground based magnetic data are provided by the Image magnetometer network [Viljanen
160 and Häkkinen, 1997; Tanskanen, 2009]. We like to note that the Image magnetic data is
161 represented in a geographically-aligned coordinate system with a North component (X), an East
162 component (Y) and a vertical Z component (positive downward).

163

164 For this study we use a particular set of data and models prepared within the EU/FP7
165 funded research project ECLAT (European CLuster Assimilation Technology program). ECLAT
166 set out to provide an unparalleled space plasma physics data repository and software tools
167 archive for Solar Terrestrial Physics, built on the existing ESA Cluster Active Archive (CAA)
168 initiative. In order to demonstrate the power of the combined space and ground-based dataset and
169 supporting modeling efforts the program carried out a number of re-analysis attempts of example
170 events, of which this study will serve as an exemplary substorm event study to be included in the
171 CAA along with other ECLAT datasets and models.

172 **3 Observations**

173 3.1 Previously reported observations

174 3.1.1 Interplanetary magnetic field conditions

175 S05 reported a well-isolated substorm on September 8th, 2002, which was preceded by a
176 long period of northward-oriented IMF, resulting in a cold, dense and thick plasma sheet
177 preceding substorm onset. A southward IMF turning occurred at the magnetopause around 2000
178 UT and the IMF turned north again around 2120UT. At around 2030UT and 2105UT, two
179 transient northward turnings of the IMF were observed by ACE and/or Wind (data not shown
180 here).

181 3.1.2 Substorm phases

182 The substorm in question is, in fact, a post-storm substorm (in the late storm recovery
183 phase), but it is well isolated from the storm active phase, both in time and in its disturbance
184 characteristics. It was observed by a radial constellation of spacecraft including Polar and Geotail
185 at X~9Re close to the plasma sheet or plasma sheet boundary layer, and Cluster at X~16Re in
186 the lobes at substorm onset. The positions of the spacecraft in the tail are shown in Figure 1, right
187 panel. Based on ground and tail data S05 found the growth phase to start at 2015 UT. The
188 substorm onset (expansion phase) was observed at ~2118 UT in the local time sector 2200-2400
189 MLT by both auroral observations of the IMAGE satellite and ground-based magnetometers in
190 Scandinavia. Figure 1, bottom panel shows the “IL” and “IU” (Image Lower and Upper) indices,
191 which similarly to the well known AL and AU indices are the negative and positive envelope
192 functions of the entire horizontal component magnetic data from the Scandinavian network. A
193 pseudobreakup was identified at 2106 UT with a weak intensity increase of the westward
194 electrojet, also accompanied by a soft plasma injection to the geostationary orbit (see S05 for

195 detail). According to S05, that pseudobreakup was probably due to either (very localized)
196 ballooning-type instability or due to the braking of a very narrow BBF.

197

198 3.1.3 Plasma Sheet Flow bursts

199 The term NFTE was introduced by *Sergeev et al.*, [1992] to emphasize the similarity
200 between dayside magnetopause FTEs (Flux Transfer Events) and BBFs in the night side plasma
201 sheet which both involve characteristics of a 3D propagation of localized reconnected flux tubes.
202 The well-known signature of an NFTE - as observed in the tail lobes - is a very asymmetric
203 bipolar B_z pattern, suggesting an open magnetic structure of the plasma and magnetic field bulge
204 associated with a B_x -compression. S05 showed that outside the plasma sheet boundary, the
205 localized bulge-like expansion of the plasma sheet traveling with the flow burst is evidenced by
206 an associated pattern of outward/inward vertical convective flows.

207 On September 8th, 2002, while in the lobes, the Cluster spacecraft encountered multiple
208 cold oxygen ion beams due to ionospheric outflow. A series of negative variations of V_z
209 accompanied by positive B_z variations (Figure 2a-2d, green shadow) suggests an association
210 between plasma tube convection toward the neutral sheet and magnetic dipolarization events.
211 S05 note “a systematic phase shift between different components: the V_z and B_z variations
212 anticorrelate each other with little phase shift evident, but the beginning of a positive δB_z
213 (negative δV_z) pulse corresponds to the maximum of B_x variation” (see S05 for detail). They
214 interpreted the quarter-period phase shift between the components as “signatures of localized
215 earthward-contracting reconnected flux tubes (NFTEs) or flux ropes”.

216 A first sequence of such NFTEs is identified during the growth phase of the substorm, in
217 the time period 2052-2105UT (Figure 2a-2d, green shadow). That these NFTEs are not observed
218 by each Cluster satellite (B_z profile differs especially at C2, not shown here) implies that they
219 are, indeed, small-scale structures traveling in the plasma sheet. A second sequence of NFTEs is
220 identified at substorm onset (around 2117UT) and throughout the substorm expansion phase. In
221 that second period, B_z and V_z vary quite similarly at both C1 and C4 (Figure 2), suggesting a
222 relatively large scale of these perturbations during this time. A delay in the magnetic signature
223 from C4 to C1 was pointed out by S05, supporting an earthward propagation of the structures.
224 From the time delay between the probes, their estimation of an earthward propagation of about
225 500-700km/s is obtained. The NFTEs identified at substorm onset by S05 are marked by the
226 vertical black dashed lines in Figure 2.

227 3.2 New observations added through ECLAT efforts

228 3.2.1 A steady westward edge of the aurora

229 Figure 3 shows the IMAGE satellite data from the proton channel of the Spectral Imager
230 (SI12, left panel) and the Wide-band imager (WIC, right panel), which is dominated by electron
231 auroral emissions [Mende et al. 2003] depicting the auroral development of the substorm (view
232 from the north-pole). First auroral intensifications are observed in the pre-midnight sector
233 starting at 2040UT, gradually establishing an active auroral oval. According to these images with
234 a 10 minutes cadence the substorm breakup takes place just before 2120 (poleward
235 intensification), consistent with the appearance of the substorm onset signatures in the
236 magnetometer and Cluster data above. A particularity of this substorm is that the substorm

237 aurora does not expand to the west, only the east. This is particularly noticeable in the IMAGE
238 FUV/WIC data (right part of Figure 3).

239 *Sergeev et al.* (1996a) demonstrated a method (inversion of mid-latitude magnetic
240 variations, [first introduced by Horning et al., \[1974\]](#), see [\[Chu et al., 2015\]](#) for the latest version)
241 in which the global distributions of bay-like perturbations in the magnetic X- and Y-components
242 observed at mid-latitude stations are fitted to the prediction from a model current system. The
243 model consists of three current systems (symmetric and partial ring currents and the SCW) and,
244 particularly, it allows inferring the total SCW current as well as the longitudes of its eastward
245 and westward edges to characterize the spatio-temporal development of substorms. The
246 reconstruction of SCW dynamics based on data from INTERMAGNET (INTERNational Real-
247 time MAGnetic Observatory NETWORK, data are available from <http://www.intermagnet.org>)
248 observations for our substorm is presented in Figure 4, where the simulated locations of the
249 upward (red) and downward (blue) FAC are displayed as a function of time and solar magnetic
250 longitude. As the timestep for the INTERMAGNET data is only 1 minute unfortunately the
251 faster fluctuations seen in the IMAGE data, which we will discuss in the following, cannot be
252 identified in this model data. Thus we only present the [longitudinal](#) development of the substorm
253 current wedge in Figure 4. The westward edge location of the SCW is clearly more or less static
254 (red points on a horizontal line) whereas the eastward edge is expanding eastward (blue points on
255 an increasing curve). Note that the longitudinal expansion of the current wedge appears to occur
256 in steps rather than in a continuous motion. One apparent large step at 2143 UT is clearly caused
257 by a lack of longitudinal data, but this lies already outside our particular period of interest for this
258 study.

259 We will later see that the lack of westward expansion quite fortuitously keeps the western
260 substorm edge (and the associated upward field-aligned current features) centered over our
261 Scandinavian network of stations, so we can follow its behavior throughout the expansion phase
262 both by Cluster in the tail and instruments on the ground. During most other substorms such
263 continuous observations are inhibited by rapid substorm expansion out of the field of view of the
264 instruments and spacecraft.

265 3.2.2 Modulation of the FAC at substorm onset

266 Localized FACs are detectable at high latitudes only indirectly via magnetic field
267 perturbations caused by ionospheric Hall currents encircling the location of the footprint of the
268 FAC, while the actual magnetic disturbances of the field-aligned currents itself below the
269 ionosphere are more or less cancelled by the magnetic effects of the ionospheric Pedersen
270 currents [*Fukushima et al.*, 1971; *Untiedt et al.*, 1978 ; *Opgenoorth et al.*, 1980; *Amm et al.*,
271 2008]. A distribution of so-called ionospheric equivalent currents can be reconstructed from
272 ground-based magnetometers. They are “virtual” currents assumed to flow only confined within
273 the ionospheric plane (assumed at 100 km altitude), but causing the same magnetic field change
274 on the ground as the real three-dimensional ionospheric/magnetospheric current system. They are
275 determined using the method of Spherical Elementary Current Systems (SECS) [*Amm and*
276 *Viljanen*, 1999; *Pulkkinen et al.*, 2003]. In these equivalent current maps/patterns a potential
277 footprint of a localized downward (upward) FAC can sometimes be identified by a quasi-circular
278 clockwise (counter-clockwise) equivalent current vortex around locations of upward (downward)
279 FAC. The analysis of such equivalent current patterns is, however, often quite difficult, as the
280 magnetic effects of newly superimposed localized field-aligned currents often are hardly visible
281 against the magnetic disturbance of the large-scale growth-phase and substorm onset electrojets.

Laurianne 14/4/2016 20:39

Deleted: latitudinal

283 Following *Untiedt et al. 1978*] and *Opgenoorth et al. [1980, 1983]*, we therefore use the
 284 method of “differential equivalent current vectors” which shows the difference in equivalent
 285 currents between the start and end time of selected intervals, which are carefully selected to
 286 represent sudden and localized occurrences of new additional current systems. Used effectively,
 287 it can be a powerful tool to visualize and understand the magnetic effect of any localized current
 288 system added to (or withdrawn from) the pre-existing background electrojets. However, the time
 289 periods for the differential current patterns have to be carefully selected to avoid a mixing of
 290 different current systems, which can lead to a completely misleading picture. In this case, for the
 291 identification of the differential intervals chosen in Figure 5, we initially inspected the
 292 “differential equivalent current patterns” from the original 10 sec resolution maps (meaning that
 293 each new equivalent current vector was reduced by the current from the preceding map, as to
 294 show only the 2-d equivalent current pattern added since the last 10 sec). Each 10 sec interval
 295 which showed a similar pattern as the preceding interval was added to the same integration
 296 period (i.e. seen as a continued addition to the same additional pattern on the original
 297 background). Only when the next 10 sec pattern showed a different or even reverse pattern, the
 298 integration was stopped and a new integration period started for as long as the basic new pattern
 299 prevailed (and so on). Any motion of the patterns during the integration times would of course
 300 lead to a blurring of the final results, but we encountered very little motion of basic patterns
 301 during this procedure. Patterns did built up for a certain time, and reversed (i.e. decreased) for
 302 another period of time. Sometimes new pattern developed slightly shifted from the patterns of
 303 previous integration periods, but any such shifts are reflected in the data shown in Figure 5.

304 Figure 5 shows the resulting differential equivalent currents (black arrows) for such
 305 selected (subsequent) intervals during the substorm onset and expansion phase. Clockwise and
 306 counter-clockwise vortices appear in the black arrow fields. As explained above, these vortices
 307 indicate the position of a downward (upward) FAC, marked on the Figure by the red (green)
 308 circle close to the center of clockwise (counterclockwise) differential equivalent current vortices.
 309 As shown in the sketch in Figure 5 (right) the Hall current vortices are not the only noticeable
 310 addition in these equivalent current patterns, but often there is an additional westward electrojet
 311 ie magnetic effects of the three-dimensional SCW are not completely cancelled. With other words
 312 in real life the Pedersen currents are not completely curl-free and the Hall currents not completely
 313 divergence-free [*Amm et al. 2008*] depending on the detailed distribution of Hall and Pedersen
 314 conductances. This additional westward electrojet superimposed on the Hall current loops results
 315 in a shift of the vortex center from west to southwest and east to northeast, and a general
 316 alignment of the westward current in a southeast- northwest direction [*Opgenoorth et al., 1980,*
 317 *Baumjohann et al.1983*].

318 Thus the red and green markings are to be understood as the “best estimated location” for
 319 the field-aligned current position (be it added or withdrawn current), which is not always at the
 320 exact center of the skewed vortex. Another problem with the Scandinavian Image dataset is the
 321 problem of boundary conditions in the eastern and western, but also north and south directions,
 322 as the number of stations outside the IMAGE network fast decreases to a few or none. Any
 323 indication of an extra rotation close to a boundary is in the SECS method closed by interpolated
 324 vectors outside the confidence area. We have taken great care not to mark any equivalent current
 325 vortices which are supported by data from less than 3 real stations (compare Figure 5 and 1).

326 From 21:18:30 to 21:25:10 UT, one can see a succession of repeated switch-ons and
 327 switch-offs (or rather partial cancellation) of additional localized current systems in the form of a

Laurianne 14/4/2016 20:42

Deleted: guess

329 current wedgelet (“ON” or “OFF” is written in the corresponding panels) with two localized
330 FACs, downward on the eastern edge and upward on the western edge. As of 21:25:10 UT and
331 onwards, mainly (only) the westward FAC is observable, because, as previously discussed, the
332 westward edge of the SCW is more or less static above Scandinavia, whereas the eastward edge
333 expands to the east, [thus the downward FAC can be outside the maps in figure 5](#). These
334 observational data from the overhead current system are consistent with the simulation of low
335 latitude data presented in Figure 4. Focusing on the westward part of the three-dimensional
336 current system, the additional upward FAC successively appears and partially disappears, which
337 can be understood as a clear modulation of the gradual built-up of the SCW. Please note that
338 during ON-periods we interpret the counterclockwise (clockwise) Hall current vortices as
339 indicators of additional upward (downward) FAC, marked with green and red circles in Figure 5.
340 During OFF-periods the corresponding colors are not indicating additional downward (upward)
341 field aligned currents in an alternating sense, but rather the disappearance of the previous pattern,
342 i.e. a switch off, or at least a partial decrease of the previously appearing SCW–onset or SCW-
343 modulation.

344 We like to point out that the identification of the “ON”, respectively “OFF” steps is most
345 clear for the first 4 or maybe 5 pulses in the magnetic field data, after which we can still see a
346 similar pattern, but occasional extra vortices do actually sometimes occur adjacent to the main
347 system. In order not to hide this effect we deliberately left one double “ON” step appear in two
348 separate integration periods (from 21:26:40-21:27:50 UT and 21:27:50-21:28:30 UT) to show
349 that deterioration of patterns for later pulses (see also 21:25:10-21:26:00 UT for an apparent
350 upward “ON” loop over Finland, which might instead be the continuation of the downward
351 “OFF” loop from the previous step, simultaneous with a new upward “ON” over Norway). We
352 attribute these deficiencies to the fact that only in the very beginning of the pulsed onset one can
353 really assume that the addition and cancellation is on a neutral background conductivity. The
354 longer we move into the process the more remnant pattern must accumulate, blurring the
355 differential vector plots. We also note that the overall character of the NFTE’s in the Cluster data
356 is most pronounced for the 4 pulses, which were already identified by S05.

357 Another way to search for possible ground signatures of localized field-aligned currents
358 is the more direct method to inspect the magnetograms from selected ground-based stations
359 equatorward from the substorm onset location. Due to curvature and inclination of the magnetic
360 field the magnetic disturbance field from the localized FACs of the SCW can readily be seen in
361 low latitude magnetometer data (or any magnetometers located sufficiently equatorward from
362 the direct magnetic effect of the circular Hall current loops typically seen at high latitudes, as
363 discussed in the previous section). At lower latitude the FAC-wedge is known to create a
364 characteristic direct disturbance field, mainly deflections in the magnetic H and D component
365 [*McPherron et al.*, 1973]. Upward (downward) FAC induces an increase (decrease) of the D
366 component which maximizes at the longitude of the FAC, and the combined current wedge
367 causes an increase in the H component, maximizing at the wedge center, at latitudes below the
368 field-aligned magnetospheric current closure paths. Figure 6 shows the IMAGE geographic East
369 component magnetograms (Y, which is equivalent to the standard magnetic D component) from
370 two sub-auroral IMAGE stations, one in the west and one in the east of Scandinavia at the
371 approximate longitudes of the initial substorm current wedge onsets (Dombas (DOB) and
372 Hankasalmi (HAN), respectively). The substorm onset is marked by a red vertical line. At DOB,
373 equatorward of the upward current location, the east component after substorm onset shows an
374 overall increase, which is a signature of the upward FAC. At HAN, equatorward of the initial

375 downward FAC location, the overall tendency after substorm onset is characterized by two
 376 successive decreases followed by an increase in the Y component. Inspecting Figure 4 we
 377 interpret this general trend as a signature of the eastward motion of the eastern edge (downward
 378 current) of the SCW. During the beginning of the event it affects HAN by a negative Y
 379 disturbance, but during the later event HAN is obviously more and more under the influence of
 380 the positive Y disturbance field of the upward field-aligned current as the downward edge moves
 381 towards the east. On top of these general trends which are in agreement with the current direction
 382 of the SCW and its subsequent eastward expansion we also note a higher frequency variation,
 383 which is observed in the data from both DOB and HAN. For closer inspection we mark in Figure
 384 6 the time intervals which correspond to an additional Hall current “ON” as determined from
 385 Figure 5. As we have discussed above, we interpret the high latitude Hall current loops as proxy
 386 observations of field-aligned current intensity modulations (switch ON and OFF). The colors are
 387 alternating pink or blue, chosen for better visibility of adjacent periods.

388 For all of these periods, the Y component at DOB (red curve) exhibits an increasing,
 389 positive pulse, i.e. an increase of upward directed FAC over the longitude of DOB. Interestingly
 390 we see that during the long “ON” interval at 21:19:50-21:21:20 UT there are two steps in the
 391 lower latitude data, which we actually on second inspection could reconfirm in the 10 sec data
 392 from the differential equivalent current vectors, but which we missed in the first analysis.
 393 Similarly the two adjacent “ON” events at 21:29:00-21:30:10 (one weak loop and one strong
 394 loop in Figure 5) seem to correspond to only one steplike enhancement of the upward field
 395 aligned current in the DOB data.

396 The Y component at HAN (blue curve) is a little more difficult to interpret, mainly due
 397 to the superimposed motion of the downward FAC to the east. However, initially we can clearly
 398 identify 3 negative pulses of the Y component disturbance field corresponding to enhancements
 399 of a downward FAC at the same longitude, when HAN is still clearly under the influence of the
 400 modulated downward portion of the SCW. Later in the event HAN mostly records positive Y
 401 pulses at the time of the “ON” modulations of the high latitude Hall current vortices, which
 402 indicates that the upward field aligned current slightly to the west of HAN has a stronger
 403 influence than the downward FAC, which is now further to the east and no longer observed by
 404 the IMAGE network.

405 **4 Discussion**

406 **4.1 Modulation of the SCW by NFTEs**

407 Based on a statistical analysis, McPherron et al. [2011] have shown that plasma flows
 408 travel with a constant velocity from -22 Re to -12 Re, then the velocity rapidly decreases to zero
 409 from -12Re to -6Re. They note that plasma flows are rarely observed inside -9Re. S05 derived an
 410 Earthward propagation velocity of the NFTEs in this event between 500-700km/s. Assuming this
 411 velocity to remain constant from the Cluster location to -12Re (respectively -9Re), will give us
 412 an estimation of when the flow could start (respectively stop) its braking phase. The onset time at
 413 Cluster of the NFTEs defined by S05 is propagated to -12 Re (marked by the leading edge of the
 414 bars on the top of figure 6), and to -9Re (marked by the trailing edge). The black (red) bars
 415 correspond to a velocity of 700km/s (500 km/s). All marks happen to be approximately at the
 416 time when an additional current is detected in the ionosphere (black or red bars for each event
 417 partially overlapping with either blue or pink color bar in Figure 6). Thus we conclude that the

Laurianne 14/4/2016 20:01

Deleted: It is of the same time scale as the NFTE sequence and the Hall current signatures at high latitude.

421 modulation of the SCW is most likely a direct consequence of the arrival of NFTE's in the near-
422 tail. One can also conclude from Figure 6 that the actual velocity of the NFTE is more likely
423 closer to 500km/s than 700km/s (producing a slightly better fit of the leading edge of the
424 rectangles).

425 The first NFTE at substorm onset is, however, quite different from all the other ones in
426 this study because it is associated with a major dipolarization/current disruption. B_z is clearly
427 higher after the NFTE passage than before the NFTE, and B_x is lower after passage than before,
428 which indicates a major energy release at this first substorm onset pulse (see Figure 2a and 2c).
429 Moreover, the decrease in the V_z velocity is far less pronounced than during the passage of the
430 other NFTEs. In Figure 6, the first sign of a SCW is identified by an increase (decrease) of about
431 10nT of the east component at DOB (HAN), which is marked by the first pink shadow. It
432 approximately corresponds to the first NFTE arrival in the near tail. Thus this first NFTE
433 containing a rather major dipolarization/current disruption is responsible for the initial creation
434 of the SCW.

435 Assuming a velocity of 500km/s from the Cluster location to the near-tail at about -12 Re
436 (where flows are expected to start braking), we can propagate backward the current wedge
437 modulation periods highlighted in Figure 6. The result is shown in Figure 2a-2d. As expected,
438 they match the NFTEs identified by S05, but they also highlight other previously not recognized
439 NFTEs. In each of these periods (pink or blue shadow), an increase of B_z and a decrease of V_z at
440 both Cluster 1 and Cluster 4 (or only one of those spacecraft) is identified.

441 So far we have induced the modulation of the substorm current wedge currents by the
442 NFTE sequence from ground-based magnetometer observations at high latitude (Hall current
443 vortices) and subauroral latitudes (direct magnetic field disturbance from FACs.) This has lead
444 us to the relation between NFTE's and FAC onsets as depicted in Figures 2 (top panels and 6).
445 Fortunately for this study Polar and Geotail are during substorm onset located at around -9Re in
446 the tail. Polar (Geotail) was in the morning (evening) sector and in the northern (southern)
447 hemisphere during the prime time of interest for this event. During the expansion phase, when
448 NFTEs were observed at Cluster, Polar measures a sequence of positive peaks in the B_y
449 component of the magnetic field (Figure 2f). Near the magnetic equator, the magnetic
450 perturbations induced by the FACs in both hemispheres can cancel each other. As Polar is
451 located slightly above the magnetic equator, the fluctuation in B_y can be interpreted as magnetic
452 effects of downward FAC (from the tail to the ionosphere) located tailward of the Polar
453 spacecraft. This result is consistent with location of the downward field-aligned current in the
454 model study of *Birn and Hesse* [2014]. Geotail, located further away from the magnetic equator
455 thus observing stronger perturbations in B_y than Polar, first observed a weak increase of B_y and
456 then pulses of decreasing B_y (Figure 2e), meaning that it was first earthward and later tailward of
457 the localized upward FAC position. The induced relative positions of the spacecraft with respect
458 to the SCW are shown in Figure 7.

459 ADDITIONALLY : So far we only discussed the pulsed intensification of the substorm
460 current wedge in response to NFTE arrival at the inner edge of the plasma sheet. We note that
461 the first sequence of NFTEs identified by S05 during this event already occurred during the
462 substorm growth phase (first green shadow in Figure 2). The ground-based magnetometers are
463 then located in the evening sector between 2200-2400 MLT. In analogy to the study by *Palin et*
464 *al.* [2015] it would be interesting to see whether also in this event the growth phase development
465 is modulated by small scale current wedgelets. Unfortunately in this case this is the region where

466 a sharp reversal of the ionospheric convection electric field can be observed, known as the
 467 Harang Discontinuity (HD) [*Kamide and Vickrey, 1983; Kunkel et al., 1986, Heppner, 1972*]. It
 468 corresponds to a convection shear zone where the eastward electrojet (equatorward of the shear)
 469 and the westward electrojet (poleward of the shear) meet. The HD is typically a source of strong
 470 and steady upward FAC. As this event was a post-storm event, the HD was clearly present and
 471 already well developed throughout the substorm growth phase. Thus it would be too complicated
 472 to analyse similar integrated differential equivalent current patterns for the NFTE influence on
 473 the growth phase current development (in the same way as we have done for the substorm onset
 474 in Figure 5).

475 Instead, we prepared a movie of the total equivalent ionospheric current over the IMAGE
 476 network from 2000 UT to 2130 UT which is presented as auxiliary material. In that movie, one
 477 can see the equivalent currents as black arrows (same as in Figure 5, but now total disturbance
 478 vectors, not differential). The background colors emphasize the areas where current is
 479 developing from weak (dark blue ~ 10 A/km) to strong (dark red ~ 3000 A/km). The color scale
 480 and exact values of the current are very dependent on the baseline definition, which in this case
 481 has been taken from a quiet day several days away from the storm period as to derive true values
 482 of magnetic disturbances caused by the substorm. Before the substorm onset, several
 483 intensifications of the ionospheric current appear as yellow areas (~ 300 A/km) in different local
 484 time (or longitude) regions. The first yellow spot, or noticeable current intensification, is
 485 observed in the time period when S05 identified NFTEs in the growth phase. Additionally, Polar
 486 observes increases of B_y at in the same time period which might be interpreted as downward
 487 FAC. As described previously, these growth phase NFTEs are small-scale structures and may not
 488 be observed by all Cluster spacecraft. Thus we might suspect in analogy of the findings by *Palin*
 489 *et al. [2015]* that the other ionospheric current intensifications during the substorm growth phase
 490 could also be triggered by NFTEs, but in a longitudinal different part of the central plasma sheet,
 491 which makes them less clearly (or not at all) detectable for the Cluster spacecraft.

492 In summary our observations show how NFTE arrival in the near-Earth tail modulates the
 493 substorm current wedge, right after substorm onset and throughout the early part of the
 494 expansion phase. In addition, we found some evidence that small SCWs are created also during
 495 the growth phase of the event in association with another sequence of NFTEs. This has in more
 496 detail been shown by *Palin et al. [2015]* for another growth phase situation before a subsequent
 497 substorm onset.

498 4.2 Relation to the coupled-mode scenario for the magnetospheric dynamics

499 It is well known that pseudobreakups can occur as substorm precursors [*Koskinen et al.,*
 500 *1993*] or as isolated events during quiet times [*Sergeev et al., 1986*], and that they show most of
 501 the signatures also found in substorms [*Ohtani et al., 1993 ; Nakamura et al., 1994*]. *Nakamura*
 502 *et al. (1994)* already noted that « *the major difference between pseudobreakups and major*
 503 *expansion onsets would be the number of (...BBF...) occurrences, as well as the intensity and*
 504 *the scale size of the magnetospheric source* ». This view is further supported by the results of
 505 *Angelopoulos et al. (1994)* that the occurrence rate of BBF increases from 6% during quiet
 506 conditions to 20% during active conditions (“active” defined as $AE \sim 500$ nT). *Sergeev et al.*
 507 *(1996b)* furthermore proposed that « *the initial breakup, the following multiple activations, the*
 508 *pseudobreakups, and other short-term activations during non-substorm times are all similar in*
 509 *morphology and have the same formation mechanism* ». Thus, they introduced the term

510 impulsive dissipation event (IDE) to describe such elementary units of energy dissipation in the
511 magnetotail. An IDE was defined as a spatially localized process with a time scale as short as
512 ~ 1 min. According to *Sergeev et al.* [1996b] “*its characteristic features are the activation (or*
513 *formation) of an auroral arc in the ionosphere, and a burst of plasma flow in the nightside*
514 *plasmashet*”. They further proposed “*two basic magnetospheric processes responsible for*
515 *energy storage and dissipation during substorms and non-substorm times: The global and*
516 *monotonic quasi-static tail reconfiguration (responsible for the energy storage and partial*
517 *release during substorm growth phase), and the multiple, local, and sporadic IDEs*”. These two
518 modes are supposed to be coupled as it is the evolution of the global mode, which in the end
519 controls the generation of IDEs.

520 Based on the discussions above we can conclude that our data and analysis presented here
521 for the first time in detail supports such general conclusions about the elementary substructure of
522 substorms, which have been presented before by other authors on the basis of less complete
523 datasets. We would like to note further that these general conclusions concerning substorm
524 growth phase and pseudobreakups have already been confirmed by *Palin et al.* [2015] with the
525 first observation of the gradual evolution of the pre-substorm ionospheric current disturbance.
526 That study also showed the relation of the number of BBFs involved in each growth phase
527 intensification to the gradual heating of the plasma sheet. At the same time the global mode is
528 affected by the integrated effects of a sequence of IDEs, thus changing the global configuration
529 of the magnetosphere.

530 *Sergeev et al.* (1996b) expressed the opinion that “*an intense substorm is simply a group*
531 *of more intense and frequent IDEs, rather than a specific entity*”. This initial conclusion was
532 based on less complete observations, but it is strongly confirmed by the present study, where
533 more intense and more frequent large-scale NFTEs are observed at substorm onset and
534 throughout substorm expansion phase, leading to the gradual built-up of a complete substorm
535 current wedge. At substorm onset the effects of a sequence of NFTEs are more dramatic and
536 have much larger amplitude as compared to a comparable, but weaker NFTE sequence during
537 the growth phase.

538 4.3 Additional understanding gained from ECLAT data and tools

539 In the following we will further elaborate how the combined usage of ECLAT tools
540 helped understanding details in this exemplary - but nevertheless complicated - case study. We
541 will show that earlier incomplete, insufficient or partial data analysis may have given rise to
542 misleading interpretations. Similar errors can certainly be extrapolated to many other substorm
543 studies in the past, which consequently may in many cases have given rise to misconceptions.

544 4.3.1 Pseudobreakup

545 The pseudobreakup at 21:06UT described in S05 was determined using a latitudinal
546 distribution of the westward currents above a meridian near midnight, derived from one
547 latitudinal profile of data from the IMAGE magnetometer network using the 1-D upward
548 continuation method (Figure 4 in S05). As discussed earlier in this manuscript, from full 2-d data
549 of the entire IMAGE network we can deduce that several small SCW occur throughout the
550 substorm growth phase, albeit at slightly varying central longitudes (and even latitudes). The
551 previously identified pseudobreakup from S05 was merely one of those small SCW which
552 happened near midnight, but it occurred exactly on the central meridian of the 1-D data analysis,

553 and thus it clearly stands out in the Figure in question. The growth phase is, however, often
 554 composed of many of such so-called pseudobreakups, but whether one will find them or not
 555 depends on where one looks and which tools are applied to display the data. Only full 2-d
 556 datasets can reveal the entire and correct picture.

557 4.3.2 Pi2 pulsations

558 Pi2 pulsations are considered to be a common signature of substorm onset. Their
 559 frequency lies between 7-25mHz (40-150s period).

560 *Keiling et al.* [2006], revisited the substorm event of S05 already before us, but in terms
 561 of understanding magnetic Pi2 pulsations. Using mostly filter techniques on space and ground
 562 based data and time-shifts between the different locations they induced a relation between tail
 563 reconnection, NFTEs, fast plasma flows, FAC and Pi2 pulsations.

564 Interpreting the NFTEs observed by Cluster as “space Pi2” sources, they [[Keiling et al.](#),
 565 [2006](#)] investigated different scenarios to explain the Pi2 propagation from Cluster location to the
 566 ionosphere (ground Pi2). Based on the Cluster data they found an Earthward propagation of the
 567 NFTEs between 600 to 800 km/s (in agreement with S05). Assuming that a NFTE is associated
 568 with a flow burst or BBF in the central plasma sheet, they used an upper limit for the velocity of
 569 1000km/s to compute a time delay to the near Earth tail at -9Re. Assuming that the flow braking
 570 would launch Alfvén waves with a velocity of 1000 km/s they found a total time delay of 98s.
 571 However, if the flow braking instead launches compressional waves with a velocity of 500
 572 km/s, they find a time delay increases to 149s. According to Keiling et al. [2006], both estimated
 573 time delays are too long compared to their observations (30s).

574 When studying Pi2 pulsations, one typically looks for fast wave propagation, i.e. either
 575 magnetosonic waves (propagating perpendicular to field-lines) or Alfvén waves (propagating
 576 parallel to field-lines). Yet, in this case study we have shown that NFTEs (signatures of a BBF
 577 traveling earthward in the central plasma sheet) occurred exactly at a similarly irregular
 578 frequency as typical Pi-2 pulsations. When braking in the near-tail they will add some currents to
 579 the already established SCW. Thus the added current to the SCW appeared in the same
 580 frequency range and the magnetic effect was observed by the ground-based magnetometers.
 581 Using simple filtering of data from individual ground-based stations apparent Pi2 pulsations can
 582 indeed be observed for extended stretches of time, however, often unexplainable phase shifts are
 583 introduced by that method, which even vary from station to station, and change with time. Our
 584 alternative explanation of such phase shifts is that the location of the field aligned current
 585 footprints moves through the network of ground-based stations, and thus any one single station
 586 will sooner or later loose synchronisation with the two-dimensional magnetic pattern. Our 2-d
 587 data in figure 5 reveals that we are instead dealing with pulses in localized Hall current structures
 588 rather than Pi-2 pulsations. This can only be resolved with a truly 2-d analysis technique as used
 589 in this study.

590 Also in accordance with the findings of *Panov et al.* [2013] (presented in the
 591 introduction), here it is the frequency (or rather sporadic periodicity) of the incoming BBFs and
 592 not their oscillatory braking which has been (mis-)interpreted as Pi2 pulsations.

Laurianne 14/4/2016 19:49

Deleted: the

Laurianne 14/4/2016 19:48

Deleted: B

595 **5 Summary and Conclusions**

596 In this study we use an event defined by S05 as “one of the best textbook examples of a
597 substorm” to investigate in more detail the relationship between NFTEs (or BBFs) and the SCW
598 development during the growth and expansion phase of a substorm. Previous studies have shown
599 that Cluster, located at about -16Re in the lobes, observes two sequences of NFTEs. The large-
600 scale NFTEs have a propagation velocity between 500-700km/s in the expansion phase of the
601 substorm.

602 The substorm onset happens right above the ground-based Image magnetometer network
603 in Scandinavia and in the close vicinity of field-lines connected to several magnetospheric
604 satellite missions. Data show that the westward edge of the SCW is more or less stable above
605 Scandinavia, whereas its eastward part is moving to the east. It means that at substorm onset and
606 throughout the early substorm expansion phase, the modulation of the upward FAC of the SCW
607 can be continuously monitored with the help of an excellent spatial coverage of ground-based
608 instruments and spacecraft.

609 This study shows that during the substorm growth phase, the NFTE arrival in the near-
610 Earth tail leads to the formation of multiple small-SCWs, which is consistent with the findings of
611 Palin et al. [2015]. However, the most important finding of this study is that even during the
612 substorm expansion phase, subsequent NFTE arrival in the near-Earth magnetotail leads to a
613 modulation (and further step-like built-up) of the SCW intensity during the expansion phase.
614 Together these intensifications build up the envelope of the magnetic disturbance pattern, which
615 is usually referred to as the “substorm bay” in a typical magnetogram. The first NFTE at
616 substorm onset is associated with a major tail current reduction/disruption, which seems to be
617 responsible for the initial SCW formation, and a first significant global dipolarisation of the
618 magnetosphere.

619 The extraordinary completeness of data for this event has already been utilized in the past
620 for a study of the transition from the growth-phase to the expansion-phase tail configuration and
621 its plasma characteristics, for the understanding of the pulsating reconnection in the tail and for
622 the understanding of onset-related Pi2 pulsations. In spite of such earlier data evaluations we
623 could show in this study how a more thorough and more complete analysis of all available data
624 and its full content could still lead to basically new results. While some of the relationships
625 identified in this paper have been postulated or shown with less complete datasets (like e.g. in the
626 paper of Juusola et al [2009]), the clear pulse-like modulation of the SCW in the early expansion
627 phase and its direct relation to the arrival of a sequence of BBFs (NFTEs) in the near-Earth tail
628 has - to the best of our knowledge - never been shown before.

629 **Acknowledgments and Data**

630 Data used in this paper were acquired by satellites operated by ESA (Cluster), NASA
631 (Polar) and JAXA (Geotail). Cluster Data were obtained through Cluster Active Archive (CAA)
632 and Geotail data from CDAWEB. We thank C. T. Russell, PI of the MFI instruments at Polar for
633 providing high resolution Polar data. Data from the NASA IMAGE spacecraft (FUV imager) has
634 been provided through the collaboration agreement within the EU/FP7 funded ECLAT project
635 and the University of Leicester, UK. We thank all the institutes, who maintain the IMAGE
636 Magnetometer Array within the MIRACLE network (at FMI Helsinki). We thank the
637 INTERMAGNET project for the magnetic observations from their mid-latitude stations.

638 LP and HO acknowledge research funding received from the Swedish National Space
639 Board, SNSB, and all co-authors acknowledge financial support for the ECLAT project from the
640 EU FP7 framework program.

641 Even though Dr. Olaf Amm (FMI) has not been an official member of the ECLAT team
642 we felt that the extensive use of his data analysis methods in this paper justified a co-authorship.
643 Due to his sudden and unexpected death in late 2014, in the middle of the finalization of this
644 manuscript, we could no longer offer him that privilege. Which is why we decided to honour his
645 valuable contributions by a special dedication of this paper to his memory, and by including him
646 as a *posthum* Co-Author, which is marked in the author-list.

647 **References**

648

649 Akasofu, S.-I. (1964), The development of the auroral substorm, *Planet. Space Sci.*, 12, 273–282,
650 doi:10.1016/0032-0633(64)90151-5.

651 Amm, O., and R. Fujii (2008), Separation of Cowling channel and local closure currents in the
652 vicinity of a substorm breakup spiral, *J. Geophys. Res.*, 113, A06304,
653 doi:10.1029/2008JA013021.

654 Amm, O., and A. Viljanen (1999): “Ionospheric disturbance magnetic field continuation from the
655 ground to the ionosphere using spherical elementary current systems”, *Earth Planets
656 Space*, 51, 431-440.

657 Angelopoulos, V., et al. (2008), Tail reconnection triggering substorm onset, *Science*, 321, 931,
658 doi:10.1126/science.1160495.

659 Angelopoulos, V., et al. (1992), Bursty bulk flows in the inner central plasma sheet, *J. Geophys.
660 Res.*, 97(A4), 4027–4039, doi:10.1029/91JA02701.

661 Angelopoulos, V., Kennel, C. F., Coroniti, F. V., Pellat, R., Kivelson, M. G., Walker, R. J.,
662 Russell, C. T., Baumjohann, W., Feldman, W. C., and Gosling, J. T.: Statistical
663 characteristics of bursty bulk flow events, *J. Geophys. Res.*, 99, 21 257–21 280, 1994.

664 Atkinson, G. (1967), An Approximate Flow Equation for Geomagnetic Flux Tubes and Its
665 Application to Polar Substorms, *Journal of Geophysical Research (Space Physics)*, 72,
666 5373, doi :10.1029/JZ072i021p05373.

667 Baker, D. N., T. I. Pulkkinen, V. Angelopoulos, W. Baumjohann, and R. L. McPherron (1996),
668 Neutral line model of substorms : Past results and present view, *Journal of Geophysical
669 Research (Space Physics)*, 101, 12,975–13,010, doi :10.1029/95JA03753.

670 Balogh, A., et al. (1997), The Cluster magnetic fields investigation, *Space Sci. Rev.*, 79,65–91,
671 doi:10.1023/A:1004970907748.

672 Balogh, A., et al. (2001), Overview of in-flight performance and initial results, *Ann. Geophys.*,
673 19, 1207–1217, doi:10.5194/angeo-19-1207-2001.

674 Baumjohann, W. (1983), Ionospheric and field-aligned current systems in the auroral zone: A
675 concise review, *Adv. Space Res.*, 2, 55–62.

676 Birn, J., M. Hesse, G. Haerendel, W. Baumjohann, and K. Shiokawa (1999), Flow braking and
677 the substorm current wedge, *J. Geophys. Res.*, 104, 19,895–19,903.

- 678 Birn, J., Raeder, J., Wang, Y.L., Wolf, R.A., Hesse, M., On the propagation of bubbles in the
679 geomagnetic tail. *Ann. Geophys.* 22, 1773 (2004)
- 680 Birn, J., and M. Hesse (2014), The substorm current wedge: Further insights from MHD
681 simulations, *J. Geophys. Res. Space Physics*, 119, 3503–3513,
682 doi:10.1002/2014JA019863.
- 683 Chu, X., et al. (2014), Development and validation of inversion technique for substorm current
684 wedge using ground magnetic field data, *J. Geophys. Res. Space Physics*, 119, 1909–
685 1924, doi:10.1002/2013JA019185.
- 686 Escoubet, C. P., M. Fehringer, and M. Goldstein (2001), The Cluster mission, *Ann. Geophys.*,
687 19, 1197–1200.
- 688 Fukushima, N. (1971), Electric current systems for polar substorms and their magnetic effect
689 below and above the ionosphere, *Radio Sci.*, 6, 269–275, doi:10.1029/RS006i002p00269.
- 690 Gibson, W.C., Burch, J.L., Scherrer, J.R., Tapley, M.B., Killough, R.L., Volpe, F.A., Davis,
691 W.D., Vaccarello, D.C., Grismore, G., Sakkas, D., Houston, S.J.: 2000, The IMAGE
692 observatory. *Space Sci. Rev.* 91(1–2), 15 – 50.
- 693 [Horning, B. L., et al. \(1974\). "Application of Linear Inverse Theory to a Line Current Model of
694 Substorm Current Systems." *Journal of Geophysical Research* 79: 5202-5210.](#)
- 695
- 696 J.P. Heppner, Electric field variations during substorms: OGO-6 measurements, *Planetary and
697 Space Science*, Volume 20, Issue 9, 1972, Pages 1475-1498, ISSN 0032-0633,
698 doi:10.1016/0032-0633(72)90052-9.
- 699 Juusola, L., R. Nakamura, O. Amm, and K. Kauristie (2009), Conjugate ionospheric equivalent
700 currents during bursty bulk flows, *J. Geophys. Res.*, 114, A04313,
701 doi:10.1029/2008JA013908.
- 702 Kamide, Y. and J. F. Vickrey, Variability of the Harang discontinuity as observed by the
703 Chatanika radar and the IMS Alaska magnetometer chain, *Geophys. Res. Lett.*, **10**, 159–,
704 1983.
- 705 Keiling, A., Fujimoto, M., Hasegawa, H., Honary, F., Sergeev, V., Semenov, V. S., Frey, H. U.,
706 Amm, O., Rème, H., Dandouras, I., and Lucek, E.: Association of Pi2 pulsations and
707 pulsed reconnection: ground and Cluster observations in the tail lobe at 16 R_E , *Ann.*
708 *Geophys.*, 24, 3433-3449, 2006.
- 709 Keiling, A., et al. (2009), Substorm current wedge driven by plasma flow vortices: THEMIS
710 observations, *J. Geophys. Res.*, 114, A00C22, doi:10.1029/2009JA014114.
- 711 Kepko, L., R. L. McPherron, O. Amm, S. Apatenkov, W. Baumjohann, J. Birn, M. Lester, R.
712 Nakamura, T. I. Pulkkinen, and V. Sergeev (2014), Substorm current wedge revisited,
713 *Space Sci. Rev.*, 1–46, doi:10.1007/s11214-014-0124-9.
- 714 Kokubun, S., T. Yamamoto, M. H. Acuna, K. Hayashi, K. Shiokawa, and H. Kawano, The
715 Geotail Magnetic Field Experiment, *J. Geomag. Geoelectr.*, 46, 7-21, 1994.

Laurianne 14/4/2016 20:37

Formatted: Font:Times New Roman, 12 pt

Laurianne 14/4/2016 20:37

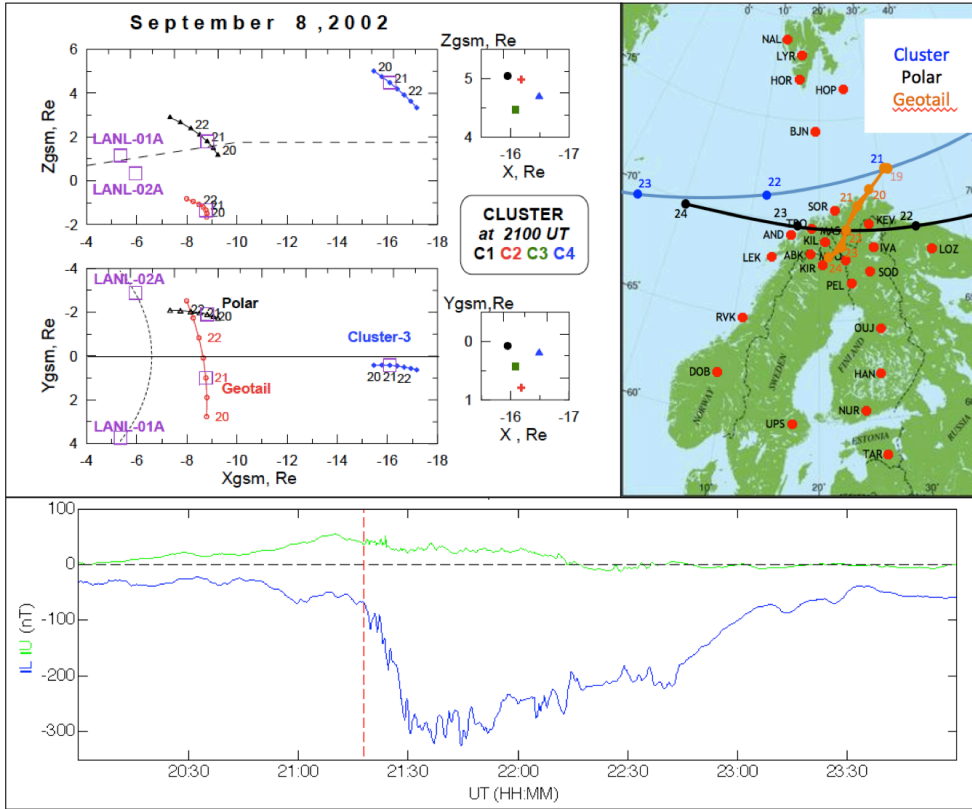
Formatted: Font:Times New Roman

- 716 Koskinen, H. E. J., R. E. Lopez, R. J. Pellinen, T. I. Pulkkinen, D. N. Baker, and T. Bösinger,
717 Pseudobreakups and substorm growth phase in the ionosphere and magnetosphere, *J.*
718 *Geophys. Res.*, **98**, 5801-5813, 1993.
- 719 Kunkel, T., W. Baumjohann, J. Untiedt, and R. Greenwald, Electric fields and currents at the
720 Harang discontinuity: A case study, *J. Geophys.*, **59**, 73-, 1986.
- 721 Liu, J., V. Angelopoulos, X.-Z. Zhou, Z.-H. Yao, and A. Runov (2015), Cross-tail expansion of
722 dipolarizing flux bundles. *J. Geophys. Res. Space Physics*, 120, 2516–2530, doi:
723 [10.1002/2015JA020997](https://doi.org/10.1002/2015JA020997).
- 724 Liu, J., V. Angelopoulos, A. Runov, and X.-Z. Zhou (2013), On the current sheets surrounding
725 dipolarizing flux bundles in the magnetotail: The case for wedgelets, *J. Geophys. Res.*
726 *Space Physics*, 118, 2000–2020, doi:10.1002/jgra.50092.
- 727 Lui, A. T. Y. (1996), Current disruption in the Earth's magnetosphere : Observations and
728 models, *Journal of Geophysical Research (Space Physics)*, 101, 13,067–13,088, doi
729 :10.1029/96JA00079.
- 730 Lui, A.T.Y., "Tutorial on geomagnetic storms and substorms," *Plasma Science, IEEE*
731 *Transactions on* , vol.28, no.6, pp.1854,1866, Dec 2000, doi: 10.1109/27.902214
- 732 Lui, A. T. Y. (2014), Evidence for two types of dipolarization in the Earth's magnetotail, *J.*
733 *Atmos. Sol. Terr. Phys.*, 115, 17–24, doi:10.1016/j.jastp.2013.10.002.
- 734 McPherron, R. L., C. T. Russell, and M. P. Aubry (1973), Satellite studies of magnetospheric
735 substorms on August 15, 1968 : 9. Phenomenological model for substorms, *Journal of*
736 *Geophysical Research (Space Physics)*, 78, 3131, doi :10.1029/JA078i016p03131.
- 737 McPherron, R. L., T.-S. Hsu, J. Kissinger, X. Chu, and V. Angelopoulos (2011), Characteristics
738 of plasma flows at the inner edge of the plasma sheet, *J. Geophys. Res.*, 116, A00I33,
739 doi:10.1029/2010JA015923.
- 740 Mende, S. B., H. U. Frey, V. Angelopoulos, and Y. Nishimura (2011), Substorm triggering by
741 poleward boundary intensification and related equatorward propagation, *J. Geophys.*
742 *Res.*, 116, A00I31, doi:10.1029/2010JA015733.
- 743 Nagai, T. (1982), Observed magnetic substorm signatures at synchronous altitude, *Journal of*
744 *Geophysical Research (Space Physics)*, 87, 4405–4417, doi :10.1029/JA087iA06p04405.
- 745 Nakamura, R., W. Baumjohann, B. Klecker, Y. Bogdanova, A. Balogh, H. Rème, J. M. Bosqued,
746 I. Dandouras, J. A. Sauvaud, K.-H. Glassmeier, L. Kistler, C. Mouikis, T. L. Zhang, H.
747 Eichelberger, and A. Runov (2002), Motion of the dipolarization front during a flow burst
748 event observed by Cluster, *Geophysical Research Letters*, 29 (20), 1942, doi
749 :10.1029/2002GL015763.
- 750 Nakamura, R., et al. (2009), Evolution of dipolarization in the near-Earth current sheet induced
751 by Earthward rapid flux transport, *Ann. Geophys.*, 27, 1743–1754.
- 752 Nakamura, R., D. N. Baker, T. Yamamoto, R. D. Belian, E. A. Bering III, J. R. Benbrook, and J.
753 R. Theall, Particle and field signatures during pseudobreakup and major expansion onset,
754 *J. Geophys. Res.*, **99**, 207-221, 1994.

- 755 Nishimura, Y., L. Lyons, S. Zou, V. Angelopoulos, and S. Mende (2010), Substorm triggering
756 by new plasma intrusion: THEMIS all-sky imager observations, *J. Geophys. Res.*, 115,
757 A07222, doi:10.1029/2009JA015166.
- 758 Ohtani, S., B. J. Anderson, D. G. Sibeck, P. T. Newell, L. J. Zanetti, T. A. Potemra, K.
759 Takahashi, R. E. Lopez, V. Angelopoulos, R. Nakamura, D. M. Klumpar, and C. T.
760 Russell, A multisatellite study of a pseudo-substorm onset in the near-Earth magnetotail,
761 *J. Geophys. Res.*, **98**, 19355-19367, 1993.
- 762 Olson, John V. Pi2 pulsations and substorm onsets: A review, *J. Geophys. Res.*, 1999 doi:
763 10.1029/1999JA900086
- 764 Opgenoorth, H. J., R. J. Pellinen, K. U. Kaila, H. Maurer, F. Kueppers, W. J. Heikkila, and P.
765 Tanskanen (1980), Ground-based observations of an onset of localized field-aligned
766 currents during auroral breakup around magnetic midnight, *J. Geophys. Z. Geophys.*, 48,
767 101–115.
- 768 Opgenoorth, H. J., R. J. Pellinen, W. Baumjohann, E. Nielsen, G. Marklund, and L. Eliasson
769 (1983), Three-dimensional current flow and particle precipitation in a westward
770 travelling surge (observed during the Barium-Geos Rocket Experiment), *J. Geophys.*
771 *Res.*, 88(A4), 3138–3152, doi:[10.1029/JA088iA04p03138](https://doi.org/10.1029/JA088iA04p03138).
- 772 Palin, L., C. Jacquey, H. Opgenoorth, M. Connors, V. Sergeev, J.-A. Sauvaud, R. Nakamura, G.
773 D. Reeves, H. J. Singer, V. Angelopoulos, and L. Turc (2015), Three-dimensional current
774 systems and ionospheric effects associated with small dipolarization fronts. *J. Geophys.*
775 *Res. Space Physics*, 120, 3739–3757. doi: [10.1002/2015JA021040](https://doi.org/10.1002/2015JA021040).
- 776 Panov, E. V., et al. (2010), Multiple overshoot and rebound of a bursty bulk flow, *Geophys. Res.*
777 *Let.*, 37, L08103, doi:10.1029/2009GL041971.
- 778 Panov, E. V., Baumjohann, W., Nakamura, R., Amm, O., Kubyshkina, M.V., Glassmeier, K.-H.,
779 Weygand, J.M., Angelopoulos, V., Petrukovich, A.A., Sergeev, V.A., Ionospheric
780 response to oscillatory flow braking in the magnetotail. *J. Geophys. Res. Space Phys.*
781 118, 1529–1544 (2013). doi:10.1002/jgra.50190
- 782 Pulkkinen, A., O. Amm, A. Viljanen and BEAR Working Group (2003): “Ionospheric equivalent
783 current distributions determined with the method of spherical elementary current
784 systems”, *J. Geophys. Res.*, 108 (A2), 1053, doi: 10.1029/2001JA005085.
- 785 Rème, H., et al. (1997), The Cluster ion spectrometry (CIS) experiment, *Space Sci. Rev.*, 79,
786 303–350, doi:10.1023/A:1004929816409.
- 787 Rème, H., et al. (2001), First multispacecraft ion measurements in and near the Earth’s
788 magnetosphere with the identical Cluster ion spectrometry (CIS) experiment, *Ann.*
789 *Geophys.*, 19, 1303–1354.
- 790 Russell, C. T., R. C. Snare, J. D. Means, D. Pierce, D. Dearborn, M. Larson, G. Barr and G. Le,
791 The GGS/Polar magnetic field investigation, *Space Sci. Rev.*, 71, 563-582, 1995.
- 792 Semenov, V. S., T. Penz, V. V. Ivanova, V. A. Sergeev, H. K. Biernat, R. Nakamura, M. F.
793 Heyn, I. V. Kubyshkin, and I. B. Ivanov (2005), Reconstruction of the reconnection rate
794 from Cluster measurements: First results, *J. Geophys. Res.*, 110, A11217,
795 doi:10.1029/2005JA011181.

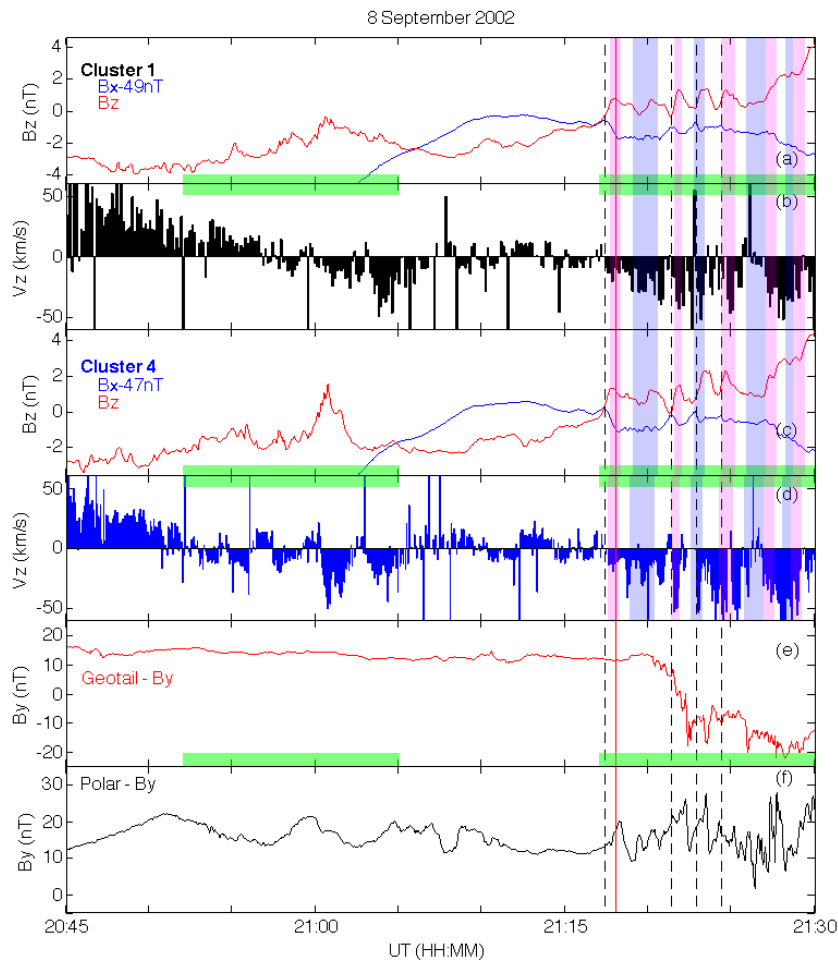
- 796 Sergeev, V. A., V. Angelopoulos, and R. Nakamura (2012), Recent advances in understanding
797 substorm dynamics, *Geophys. Res. Lett.*, 39, L05101, doi:10.1029/2012GL050859.
- 798 Sergeev, V. A., I. A. Chernyaev, V. Angelopoulos, A. V. Runov, and R. Nakamura (2014),
799 Stopping flow bursts and their role in the generation of the substorm current wedge,
800 *Geophys. Res. Lett.*, 41, 1106–1112, doi:10.1002/2014GL059309.
- 801 Sergeev, V., Elphic, R. C., Mozer, F. S., Saint-Marc, A., and Sauvaud, J.-A.: A two-satellite
802 study of nightside flux transfer events in the plasma sheet, *Planet. Space Sci.*, 40, 1551–
803 1572, 1992.
- 804 Sergeev, V. A., Kubyshkina, M. V., Baumjohann, W., Nakamura, R., Amm, O., Pulkkinen, T.,
805 Angelopoulos, V., Mende, S. B., Klecker, B., Nagai, T., Sauvaud, J.-A., Slavin, J. A., and
806 Thomsen, M. F.: Transition from substorm growth to substorm expansion phase as
807 observed with a radial configuration of ISTP and Cluster spacecraft, *Ann. Geophys.*, 23,
808 2183–2198, 2005,
- 809 Sergeev, V. A., A. G. Yahnin, R. A. Rakhmatulin, S. I. Solovjev, F. S. Mozer, D. J. Williams,
810 and C. T. Russell, Permanent flare activity in the auroral zone, *Planet. Space Sci.*, 34,
811 1169–, 1986.
- 812 Sergeev, V. A., L. I. Vagina, R. D. Elphinstone, J. S. Murphree, D. J. Hearn, L. L. Cogger, and M.
813 L. Johnson (1996a), Comparison of UV optical signatures with the substorm current
814 wedge as predicted by an inversion algorithm, *J. Geophys. Res.*, 101, 2615–2627,
815 doi:10.1029/95ja00537.
- 816 Sergeev, V. A., T. I. Pulkkinen, and R. J. Pellinen (1996b), Coupled-mode scenario for the
817 magnetospheric dynamics, *J. Geophys. Res.*, 101(A6), 13047–13065,
818 doi:[10.1029/95JA03192](https://doi.org/10.1029/95JA03192).
- 819 Troshichev, O. A., B. M. Kuznetsov, and N. P. Dmitrieva (1979), Polar cap magnetic activity as
820 a signature of substorm development, *Planetary and Space Science*, 27, 217–221, doi
821 :10.1016/0032-0633(79)90063-1.
- 822 Tanskanen, E.I. (2009), A comprehensive high-throughput analysis of substorms observed by
823 IMAGE magnetometer network: Years 1993-2003 examined, *J. Geophys. Res.*, 114,
824 A05204, doi:10.1029/2008JA013682.
- 825 Untiedt, J., R. Pellinen, F. Küppers, H. J. Opgenoorth, W. D. Pelster, W. Baumjohann, H. Ranta,
826 P. Kangas, P. Czechowsky, and W. J. Heikkila (1978), Observations of the initial
827 development of an auroral and magnetic substorm at magnetic midnight, *J. Geophys.*, 45,
828 41–56.
- 829 Viljanen, A., and L. Häkkinen (1997), IMAGE magnetometer network, in *Satellite-Ground
830 Based Coordination Sourcebook*, edited by M. Lockwood, M. N. Wild, and H. J.
831 Opgenoorth, Eur. Space Agency Spec. Publ., ESA-SP1198, 111
832

833
834



835
836

837 **Figure 1.** Left panel: Figure from S05 : Configuration of basic spacecraft positions on 8
838 September 2002 in GSM-coordinates. The neutral sheet position is indicated on the XZ cross
839 section, spacecraft positions at 2100 UT are marked by rectangles. Right panel: Footprints of
840 Cluster, Polar and Geotail spacecraft obtained from the model by Tsyganenko et al. [1989] and
841 location of ground-based magnetometers from the IMAGE network. Bottom : IL and IU indices,
842 red vertical line mark the substorm onset.
843
844

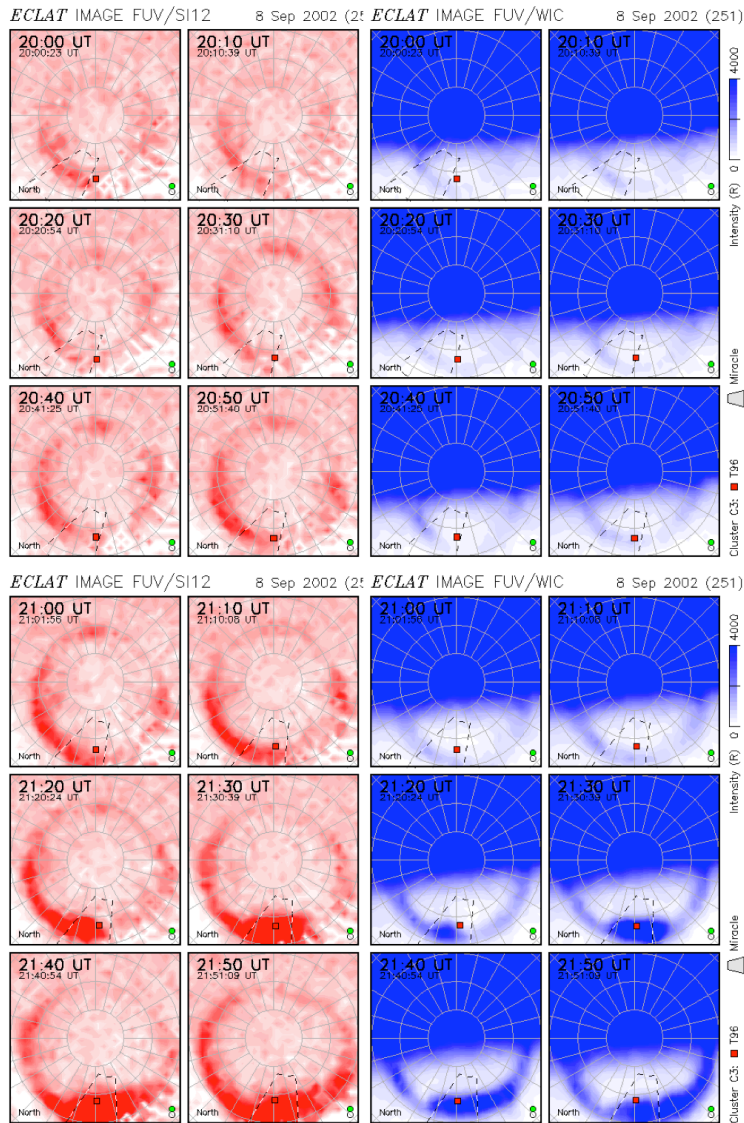


845

846 **Figure 2.** Upper 4 panels: Bx (adjusted by a constant offset to be plotted together with Bz) and
 847 Bz variations (a and c) and O⁺ perpendicular flows (b and d) at C1 and C4 spacecraft. Lower
 848 panels: By-variations at Geotail (e) and Polar (f) spacecraft. The coordinate system used in this
 849 picture is GSM. Green shadows : periods of NFTEs identified by S05. Red solid line : substorm
 850 expansion phase onset (from S05). Black dashed line: NFTEs around substorm onset, at Cluster
 851 (from S05). Pink and Blue shadows explained in text.

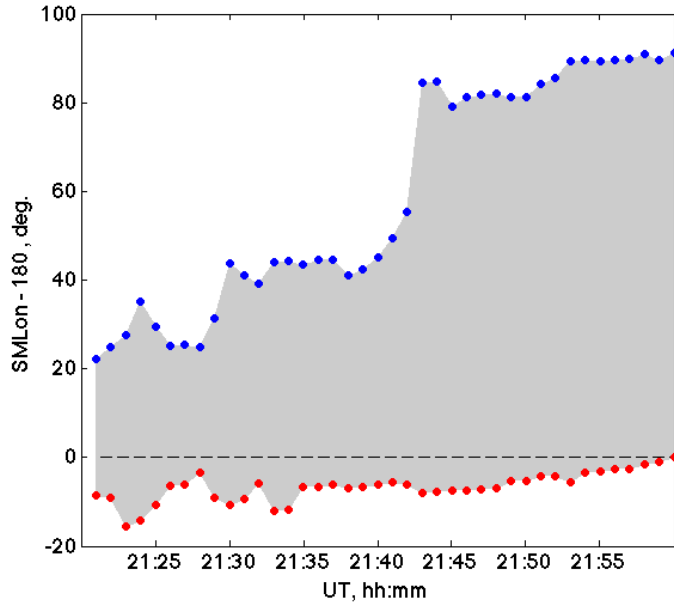
852

853



854

855 **Figure 3.** Image satellite global view of the auroral development at two different wavelengths
 856 depicting proton aurora (SI12) on the left and wideband emissions from mainly electron aurora
 857 on the right (WIC) from 2000UT to 2200UT. The red square marks the footprint of Cluster 3
 858 location. The area in the dashed lines is the location of Miracle network. The two circles at the
 859 bottom right of each plots are quality flags, green means good quality data.
 860
 861



862

863 **Figure 4.** Simulation of the SCW using the model of Sergeev et al. (1996a), see text for
 864 explanation. To is the time of substorm onset in the model. The position of the FAC flowing
 865 down (out) to the ionosphere is in blue (red), SMLon is the longitude in the Solar Magnetic
 866 coordinate system.

867

868

869

870

871

872

873

874

875

876

Laurianne 25/4/2016 17:14

Deleted: : PE (PW)

Laurianne 25/4/2016 17:14

Deleted: .

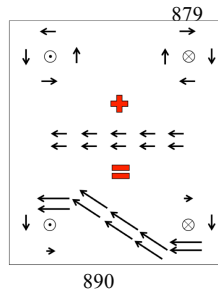
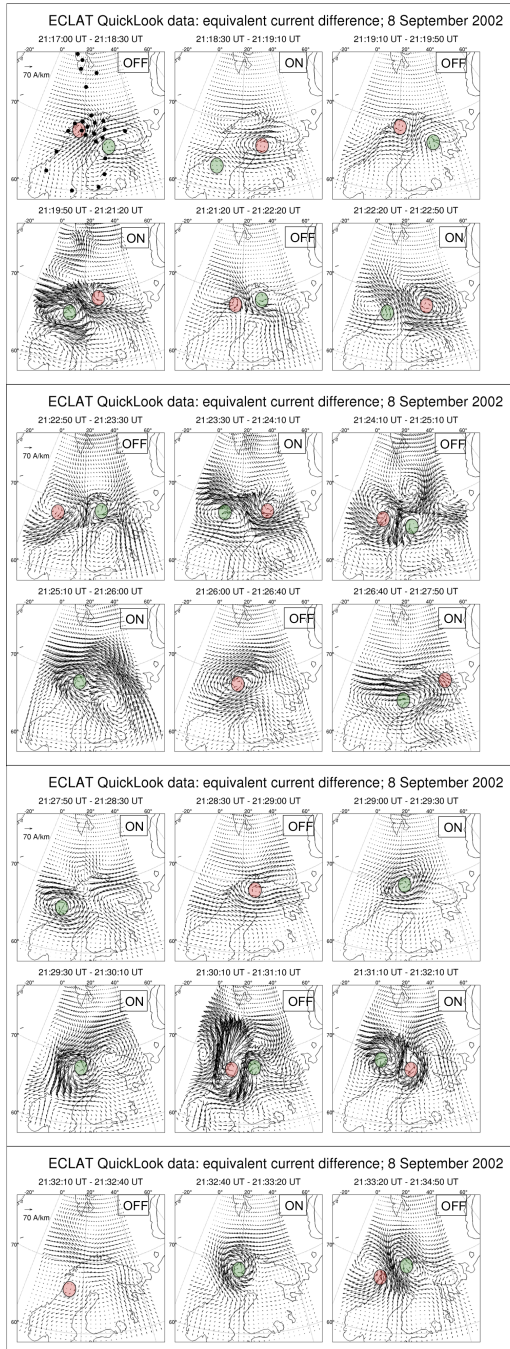
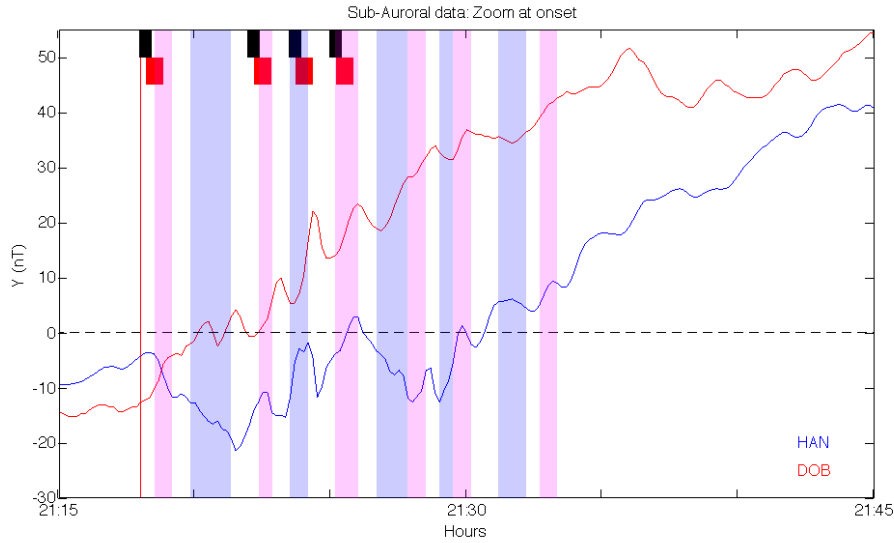


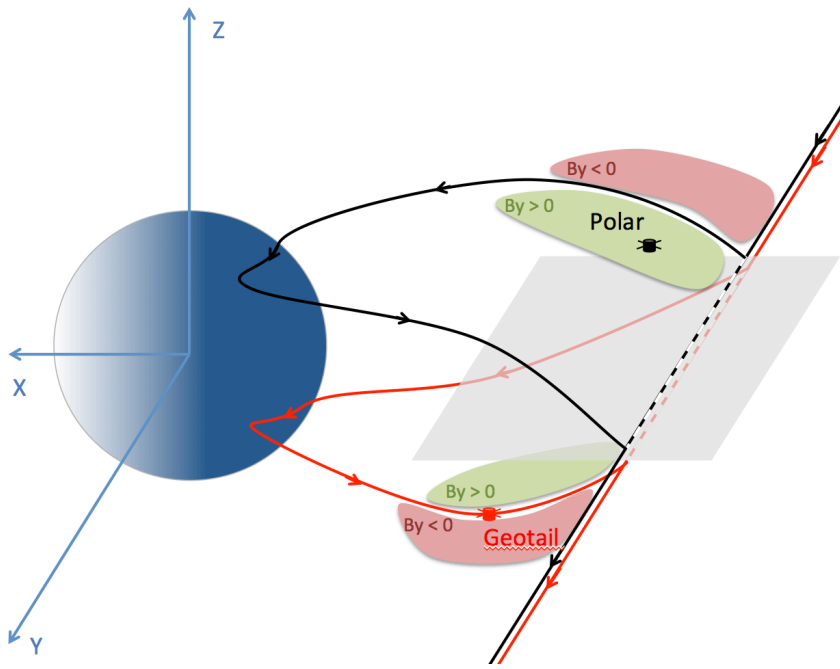
Figure 5. Left Panels: “Differential equivalent current vectors” showing the difference in equivalent currents between the start and end time of selected intervals i.e. the magnetic effect of any additional current system added to (or withdrawn from) the pre-existing large scale background electrojets. [The black dots on the first panel shows the location of ground based magnetometers.](#) Insert on top right: sketch of the total equivalent current distribution current distribution when adding a westward electrojet to the circular Hall current patterns encircling the footprints of field aligned currents, see text.

908



909

910 | **Figure 6.** Ground based magnetometer data from two subauroral stations of the Image
 911 magnetometer network – geographic East components of HAN and DOB - around and after
 912 substorm onset. (for exact station location see figure 1). Red solid line : substorm expansion
 913 phase onset (from S05). Pink and blue shadow (two colors used for better visibility of adjacent
 914 periods): Time period where SCW modulation is “ON” in figure 5. The rectangles on top of the
 915 plot marks the expected time period of flow braking in the region from -12 to -9 R_e , assuming a
 916 propagation velocity of 700km/s (black) and 500km/s (red). See text for detail description.
 917



918

919 **Figure 7.** Sketch of the SCW and the position of Polar and Geotail spacecraft relative to the
920 localized FACs in both hemispheres (black north, red south), and on the evening side (upward
921 currents) and morning side (downward currents) of the SCW.
922

923